

Bioinspired Multi-Layer Biopolymer-Based Dental Implant Coating for Enhanced Osseointegration

Betul Uzulmez, Zeynep Demirsoy, Ozge Can, and Gulcihan Gulseren*

The major drawbacks of metal-based implants are weak osseointegration and post-operational infections. These limitations restrict the long-term use of implants that may cause severe tissue damage and replacement of the implant. Recent strategies to enhance the osseointegration process require an elaborate fabrication process and suffer from post-operative complications. To address the current challenges taking inspiration from the extracellular matrix (ECM), the current study is designed to establish enhanced osseointegration with lowered risk of infection. Natural biopolymer pectin, peptide amphiphiles, and enzyme-mimicking fullerene moieties are governed to present an ECM-like environment around the implant surfaces. This multifunctional approach promotes osseointegration via inducing biomineralization and osteoblast differentiation. Application of the biopolymer-based composite to the metal surfaces significantly enhances cellular attachment, supports the mineral deposition, and upregulates osteoblast-specific gene expression. In addition to the osteoinductive properties of the constructed layers, the inherent antimicrobial properties of multilayer coating are also used to prevent infection possibility. The reported biopolymer-artificial enzyme composite demonstrates antimicrobial activity against *Escherichia coli* and *Bacillus subtilis* as a multifunctional surface coating.

serious effects compromise their usage.^[2] The major concerns with these implants are persistent infections and poor osseointegration, and these handicaps could eventually cause severe tissue damage and replacement of the implants. To prevent infection in the short-term as well as ensure successful long-term attachment of the implant to native tissue, proper early-phase management of scar tissue is crucial.^[3,4] Most of the past and current research has concentrated on the modification of surface properties of bone implants with minerals, antibiotics, polymers, and bioactive reagents.^[5] Unfortunately, these techniques usually necessitate laborious fabrication processes and are often dependent on costly materials with low stability. As an alternative solution, extracellular matrix (ECM) mimicking materials with antimicrobial characteristics have been explored – offering a suitable platform for stimulating cellular responses and decreasing the risk of infection.^[6] This study uses pectin, peptide (K-PA), and enzyme-mimicking nanocatalysts (F-His-Thr) as three main ingredients of a cell matrix (proteins, polysaccharides,

and enzymes) as a practical coating approach for implants; thereby overcoming current shortcomings of prior practices.

Due to its biocompatibility and adhesive features, as well as its broad-spectrum antimicrobial properties,^[7] pectin is often seen as a great candidate for biomimetic systems.^[8,9] Its microenvironment also has advantages for cell growth, proliferation, and differentiation making it a sought-after choice for tissue regeneration projects.^[10,11] Yet, the high carboxyl content of this natural polysaccharide results in inadequate surface features for cellular attachment. To tackle this issue, integrin-binding peptides have been used to modify pectin molecules.^[12] However, these methods are time-consuming and can cause toxic byproducts.

Non-covalent cross-linking is a promising strategy to modify the physical, chemical, mechanical, and even biological features of biopolymer films.^[13] The technique of peptide-aided cross-linking of biopolymers has been established as an effectual method to refine the physical, chemical, and biological properties of biopolymers.^[14,15] Self-assembled peptide nanofibers are recurrently adopted to replicate ECM. Their flexible nature allows for customizing their structural composition and chemical attributes while manipulating biological responses. By non-covalent alteration of pectin biopolymer with a combination of


1. Introduction

Metal-based implants have been routinely used for clinical trials due to their outstanding physical features.^[1] Generally, these implants contain titanium and stainless-steel, which are biologically inert. However, postoperative complications that can lead to

O. Can, G. Gulseren
Department of Molecular Biology and Genetics
Konya Food and Agriculture University
Konya 42080, Turkey
E-mail: gulcihan.gulseren@gidatarim.edu.tr

B. Uzulmez, Z. Demirsoy, G. Gulseren
Department of Biotechnology
Konya Food and Agriculture University
Konya 42080, Turkey

O. Can
Department of Bioengineering
Izmir Institute of Technology
Izmir 35430, Turkey

 The ORCID identification number(s) for the author(s) of this article can be found under <https://doi.org/10.1002/mabi.202300057>

DOI: 10.1002/mabi.202300057

nanofibers, bioactive nanoscale matrices can be created. Thus, pectin's physical properties can be customized for enhanced cell adhesion and biomineralization for osteogenic differentiation. Herein, a bioactive adhesive peptide amphiphile was chosen for this purpose. This method provides versatility in designing the desired biological response based on the modification of pectin biopolymer strands. The basement layer of our composite is constructed by crosslinking these biopolymers.

The final element of the recent study is an enzyme mimic, which was incorporated as the top layer in order to serve as a promoter of osseointegration and biomineralization. Phosphatases play an essential role in bone regeneration and their external administration advances the formation of such tissues.^[16,17] While these enzymes are widely employed in osteoregeneration studies, low-stability problems must be solved in order to enable long-term bioactivity.^[18] Synthetic enzymes have thus emerged as a viable and multifunctional alternative to natural ones.^[19] Recently, fullerene has been recognized as a powerful artificial enzyme-mimicking tool due to its surface characteristics and biocompatible nature.^[17,20–22] To this end, histidine and threonine functionalized fullerene nanoparticles (HT) have been utilized for phosphatase activity. The study from our group further demonstrated the phosphatase-mimicking capacity of such nanocatalysts with tunable bioactivity for both phosphomonoesterase and phosphodiesterase substrates (Figures S3 and S4, Supporting Information). Similar to the natural counterpart, which mineralizes the collagen matrix, these nanocatalysts produce inorganic phosphates to support the biomineralization of nano matrices. In addition to enzyme activity, HT has shown antibacterial activity against gram-negative *Escherichia coli* (*E. coli*) and gram-positive *Bacillus subtilis* (*B. subtilis*) among the other fullerene derivatives (Figure S5, Supporting Information).

The objective of this study is to develop a novel multifunctional interface for metal-based implants that can promote cell attachment, biomineralization, and osteogenic differentiation, while simultaneously reducing the risk of postoperative complications. Our attention was directed toward establishing sufficient osseointegration in the initial stage and addressing early-phase concerns that contribute to long-term success. The ECM-mimicking coating is made using pectin, peptides, and fullerene-based nanocatalysts, and is formed through non-covalent cross-linking of pectin biopolymer strands with a bioactive adhesive peptide amphiphile and enzyme-mimicking nanocatalysts. This approach provides versatility in designing the desired biological response based on modification of pectin biopolymer strands, without relying on chemical modifications that can produce toxic byproducts. By utilizing enzyme-mimicking nanocatalysts together with a pectin-peptide fibrous network, an undocumented implant coating platform has been created that promotes both osseointegration and biomineralization.

The significance of designing such a coating lies in its ability to address the challenges associated with metal-based implants, such as persistent infections and poor osseointegration. By using materials that mimic the extracellular matrix and have antimicrobial properties, this coating offers a suitable platform for stimulating cellular responses and decreasing the risk of infection. Moreover, the use of non-covalent cross-linking provides a practical and cost-effective method for modifying the physical, chemical, mechanical, and biological features of biopolymer films. By

providing a multifunctional interface, this coating aims to improve adhesion between the implant and cell interface, reducing adverse effects associated with implant applications.

2. Results and Discussions

2.1. Characterization of Surface Coatings

Pectin or peptide-based biomaterials have been widely used in tissue engineering applications due to their biocompatibility, biodegradability, modifiability, and low cost.^[10,23] To generate an interface between tissues and implant surfaces, the surface coatings' physical properties must be considered carefully to develop bilateral adhesiveness. In recent studies, catechol^[24] and RGD motifs^[14,25] were commonly employed to design adhesive coatings due to their strong surface binding properties. Herein, we propose a new approach to generate multifunctional surface coating without requiring costly chemical cross-linking or modification. To combine desirable features in a simple procedure, a non-covalently cross-linked pectin/peptide/nanocatalyst composite was used to construct these multifunctional interfaces and the properties of this recent composite were investigated.

The bioactive peptide sequence (lauryl-VVAGK-Am) was synthesized using the solid phase synthesis technique. This sequence is adopted from previous work^[16] with a lysine group to improve non-covalent cross-linking between carboxyl groups of the pectin biopolymer. Another reason for the selection of the lysine residue is its potential antimicrobial activity due to the multiple presentations of lysine residues on peptide nano surfaces, similar to the antimicrobial action of Poly-L-Lysine. In addition to utilizing nanofiber-based cross-linking, the technique of cross-linking with peptide nanofibers was employed to improve cellular attachment by increasing the branching sites of the pectin and creating a bioactive sequence that encourages osteoregeneration.^[14] The purity of peptide amphiphiles is characterized by liquid chromatography and mass spectrometry method (LC-MS) (Figure S1, Supporting Information). Fullerene nanocatalyst was synthesized using the previously reported method^[20] and characterized by proton nuclear magnetic resonance (¹H-NMR), elemental analysis, and high performance liquid chromatography (HPLC)-based amino-acid quantification methods (Figure S2, Supporting Information).

For the fabrication of bioactive surfaces, as illustrated in **Figure 1**, peptide-pectin complex (PP) was coated onto stainless steel or glass surface, and this process was followed by a second layer coating with the fullerene-based enzyme mimic (HT), and the complete layers were formed (HT-PP). The non-covalent interactions of pectin polymer chains with peptide amphiphiles caused fibrous network formation similar to ECM. Fibrous entanglements resembling ECM-like networks were visualized by scanning electron microscopy (SEM). The non-covalent modification of pectin with peptide amphiphiles was evaluated by Fourier transform infrared (FTIR) spectroscopy. In the analysis of only pectin, the absorption bands at nearly 1736 and 1613 cm⁻¹ can be attributed to the C = O of the methyl ester group and undissociated carboxylic acid.^[26] With the addition of the peptide, these pectin-specific peaks shifted toward 1634 and 1541 cm⁻¹, containing the contribution of C = O stretching and N-H bending of

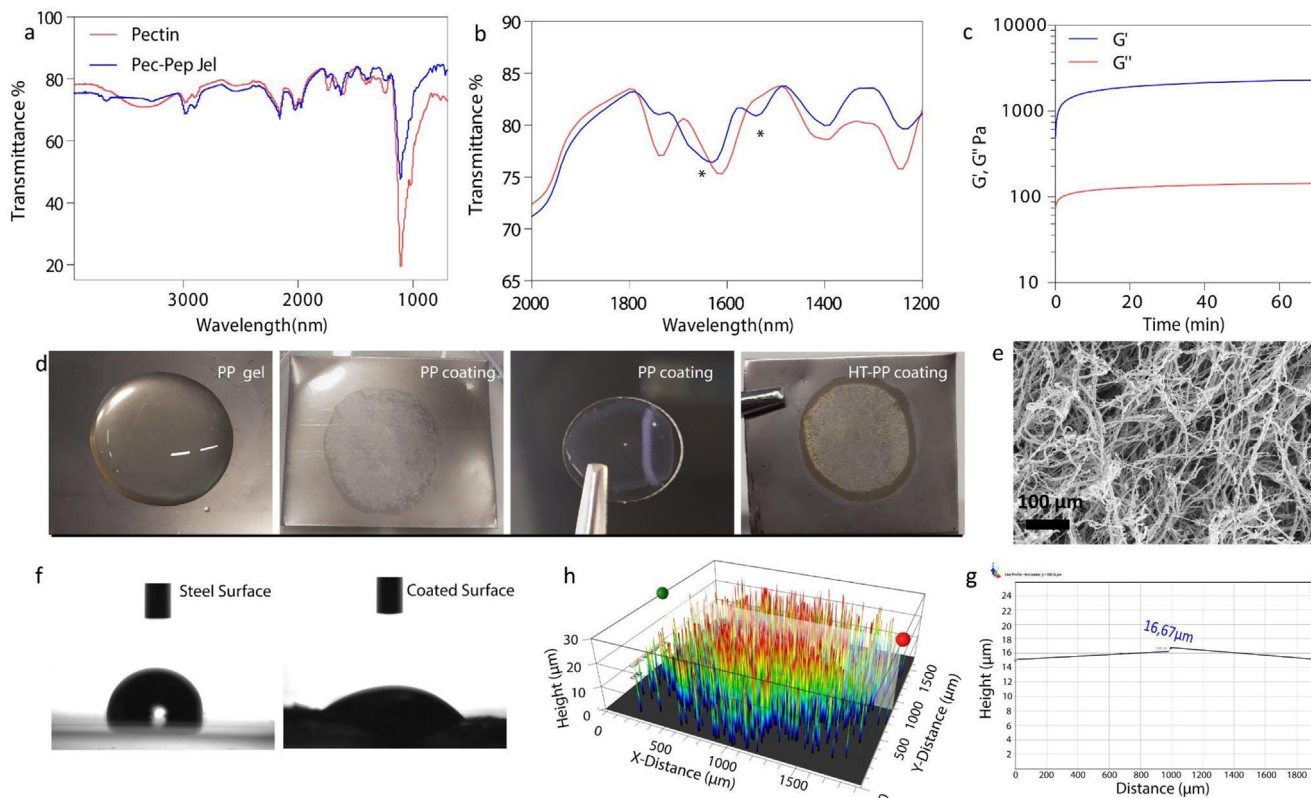


Figure 1. a) Complete spectra of FTIR of pectin and PP gel. b) Indication of spectral shifts induced with the introduction of the peptide. c) Rheometer time sweep measurements of PP gel. d) Illustration of coatings on stainless steel and glass surface with PP gel and HT-PP. e) SEM image of PP fibrous network (scale bar 400 μm). f) Contact angle analysis of steel surface before and after coating h) Optical profilometer analysis indicating surface topography and g) thickness measurement.

peptide amphiphiles (Figure 1). These absorption peaks appeared due to the presence of peptide moieties. These emerging peaks could be assigned to non-covalent interaction among pectin and peptide fibers, leading to fibrous network formation.

The adsorption of peptide-pectin gel was primarily inspected by the optical profilometry technique. Due to their exceptional biocompatibility, most currently available dental implants are made from stainless-steel-based materials. Coated stainless-steel surfaces were evaluated after repetitive washing, and optical profilometry analysis revealed that the thickness of the coating is $\approx 16 \mu\text{m}$ (Figure 1).

Changes in the surface hydrophobicity upon loading multiple bioactive components on stainless steel surfaces were investigated by contact angle measurements. The contact angle of the stainless-steel surface was measured to be $106.14 \pm 2^\circ$, and the coated surface radically decreased the contact angle value below $42.96 \pm 0.7^\circ$ (Figure 1). This observation can be explained by the highly hydrophilic and porous physical characteristics manifested by the fibrous surfaces of the adsorbent pectin-peptide network. The formation of the hydrogel ($G' > G''$) was studied by oscillatory rheology, and viscoelastic properties of the formed network were identified. Rheometer measurements of pectin-peptide further confirmed the formation of a hydrogel stabilized by the physical entanglement of pectin and peptide nanofibers.

The stability of the new coating method was tested on different surfaces. Steel, glass, and polymer surfaces were coated with

multilayer coatings and the coated surfaces were incubated in 1x PBS for 15 days to mimic the swelling behavior of the coating in tissue after implantation. When the percent weight loss was calculated, it was found that coatings retained more than half of their weight for all surface types, and the highest stability was observed for the coating on the glass surface with almost 3% weight loss (Table S1, Supporting Information). Moreover, in the stability test made with swimming polymeric mold enabling the contact of the liquid from both sides of the multilayer coating (Figure S6, Supporting Information), coatings protected more than 70% of their weight. Since the early stage osseointegration occurs during the first week with the events of osteoblast differentiation, production of osteogenic factors, cytokines, and growth factors.^[27] The observed stability values on different surfaces are satisfactory to promote the osseointegration at the early stage.

2.2. Induction of Biomineralization

Dental coatings were designed to induce biomineralization on implant surfaces to improve osseointegration via supporting mineralized tissue formation on the defect site. To enhance the generation of inorganic phosphate, implant coating was designed using layers of pectin-peptide and threonine/histidine-modified fullerene. The coating incorporated HT as an enzyme-like compartment, and its catalytic efficiency was evaluated. Surprisingly,

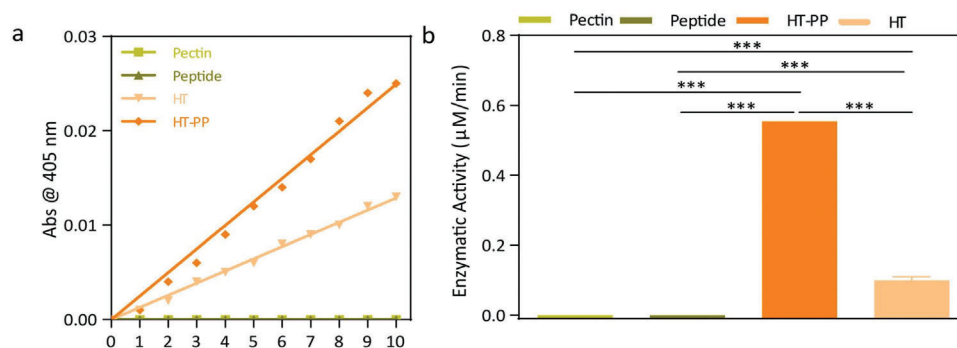


Figure 2. Phosphatase activity on HT-PP coated surfaces. Illustration of comparative catalytic profile analysis of pectin, peptide, HT, and HT-PP (Mean \pm SEM, $n =$ at least 2, one-way analysis of variance (ANOVA); * $p < 0.0332$, ** $p < 0.0021$, *** $p < 0.0002$, **** $p < 0.0001$).

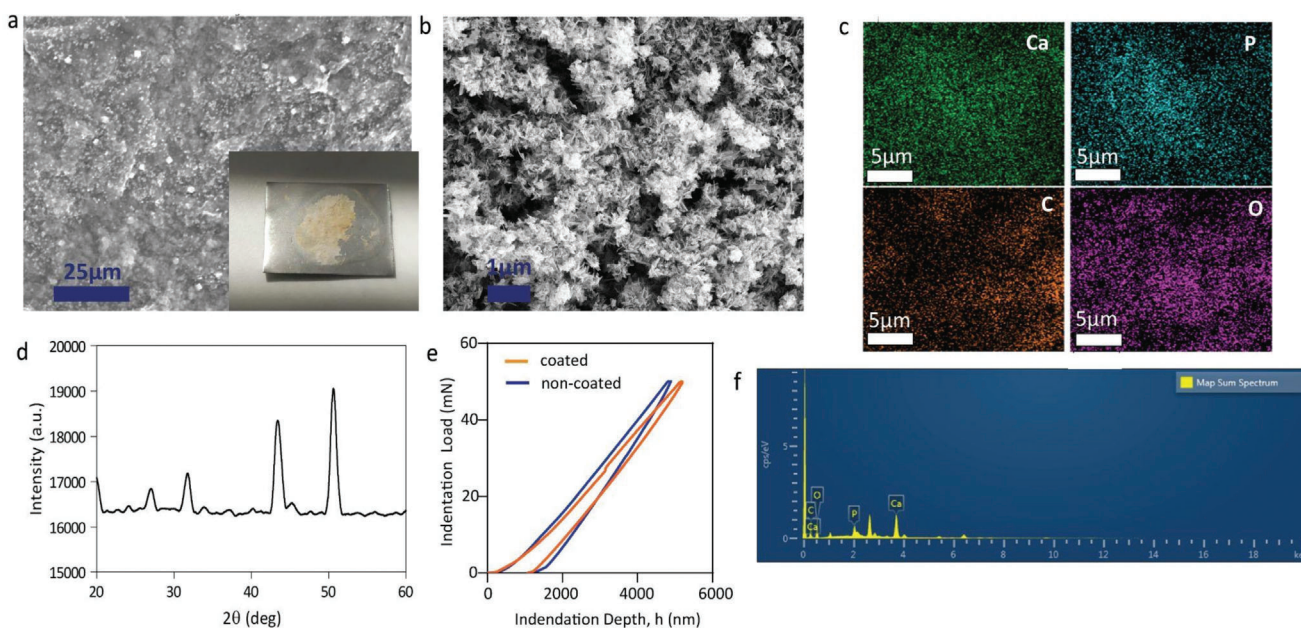


Figure 3. CaP deposition on HT-PP coated surfaces. a) Illustration of mineralized coatings (coated on stainless-steel surface) and SEM image of the mineralized surface showing CaP deposition. b) Structure of the formed mineral crystals with SEM. c) EDX mapping of mineral content on coated surfaces. d) XRD diffractogram of deposited minerals. e) Loading and unloading nanoindentation curves of coated and non-coated steel surfaces. f) EDX analysis of formed crystals for elemental identification.

the complete coatings (HT-PP) demonstrated a superior catalytic profile compared to HT, while the control groups did not exhibit any catalytic activity (Figure 2). The improved inorganic phosphate cleavage observed in the HT-PP coatings may be attributed to the presence of additional carboxyl and amine groups on the gel surface, as well as the attachment of enzyme-like moieties to the fibrous network.

To investigate the mineralization capacity, the coated surfaces were incubated in a natural salt environment. Following this process, the surfaces were washed to remove soluble minerals. The deposited minerals on coated stainless-steel surfaces were evaluated with SEM microscopy and energy-dispersive X-ray (EDX) analysis. The physical appearance of formed biomaterials on coated surfaces was visualized by SEM, and calcium phosphate (CaP) like morphology was observed. EDX analysis and mappings illustrated that coated surfaces successfully induced

CaP formation (Figure 3). Crystal structure analysis of deposited minerals was performed by X-Ray diffraction (XRD). Obtained XRD diffractogram revealed hydroxyapatite (HA) and tricalcium phosphate (β -TCP) specific patterns, the peaks were obtained at $2\theta = 26.8^\circ$ (002), 31.6° (211), 43.4° (202) and 50.7° (402). All the diffraction peaks shifted slightly due to the polymer attachment and loss of crystallinity of HA material.^[28] These patterns were identified with the joint committee on powder diffraction standards (JCPDS) cards 00-09-0432 for HA and 01-070-2065 for β -TCP.^[29,30] Amorphous nature of deposited minerals was illustrated with microscope images and XRD analysis.

Utilizing the nanoindentation technique, the mechanical properties of coated surfaces at the nano-scale were analyzed. The findings indicate that the coated surfaces containing mineralized coatings exhibited greater plastic deformation compared to their non-coated counterparts, owing to their relatively softer

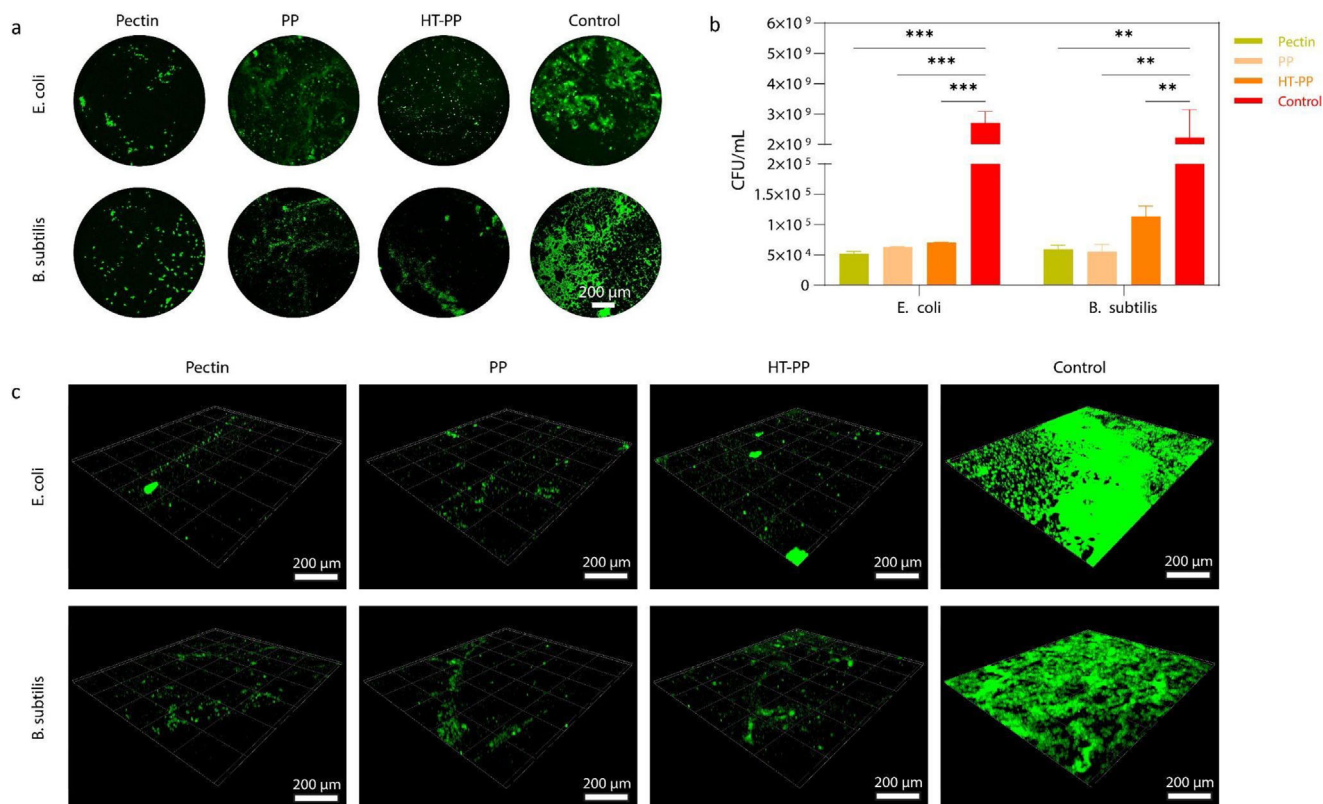


Figure 4. a) After overnight incubation of *E. coli* and *B. subtilis* with pectin, PP, HT-PP, and collagen control. Samples were fixed with 4% PFA and observed under a fluorescence microscope at 10× magnification. The bacterial cells were stained with crystal violet. b) The graph shows bacterial growth at CFU/mL after overnight incubation with described conditions (Mean ± SEM, $n = 2$, two-way analysis of variance (ANOVA); * $p < 0.0332$, ** $p < 0.0021$, *** $p < 0.0002$, **** $p < 0.0001$). c) 3D Z-Stack image of the fluorescent bacterial samples taken with 12 μm depth.

composition. As evidenced in Figure 3e, the coated samples showed a permanent deformation of roughly 5200 nm, while the steel surface experienced a deformation of ≈ 4800 nm. The modulus of the coated samples and steel surface was determined by computing the slope of the unloading curve to be 4.93 ± 0.03 and 7.24 ± 0.05 GPa, respectively. The increased plastic deformation in the coated samples was attributed to the mineralized coatings' brittle nature.

2.3. Prevention of Bacterial Growth

To assess the antimicrobial capacity of HT-PP coatings, coated surfaces were exposed to two different bacterial strains. Bacterial strains, *E. coli* and *B. subtilis*, were selected as representatives of gram-negative and gram-positive bacteria, respectively. These strains are commonly found in foods and can exhibit different levels of pathogenicity. *E. coli* and *B. subtilis* can be found in the gastrointestinal tract of humans^[31] so, with the food, they can also be infectious, especially if contaminated food is raw, undercooked, or unpasteurized. Thus, the oral cavity is at high risk of infection. The risk is much higher with conventional dentures and oral implants since they have a suitable material surface for bacterial growth.

The antibacterial activity of three experimental groups, pectin, PP, and HT-PP was assessed with a new method that mimics

the 3D environment of the dental tissue. In this method, coatings were prepared inside molds that swim in a medium^[32] (Figure S6, Supporting Information), enabling a dynamic environment for the bacterial cells together with the rotational motion throughout the incubation. This dynamic environment simulates the changing mechanical pressures applied to dental tissue. As a control group, we used collagen, which is the major ECM component where bacterial cells attach and grow. According to alamarBlue viability results, all of the experimental groups (pectin, PP, and HT-PP) illustrated significant antibacterial activity for both gram-negative and gram-positive strains, and there were no significant differences among the antibacterial activity of those groups (Figure 4). Almost 10^5 -fold-decreased colony forming unit (CFU) number was obtained for the pectin, PP, and HT-PP compared to collagen control for both bacterial strains. However, the decrease was more drastic for *E. coli*, which could mean that our multilayer coating is more effective for gram-negative strains. Results show that coatings have an antimicrobial effect, not via strong bactericidal activity but rather by inhibiting microbial cell growth.

HT-PP coating, with significant antibacterial activities for both gram-negative and gram-positive strains, presents the potential for clinical use, considering the initial number of bacteria (1×10^6 CFU/well) used in the assay is much higher than the number of bacteria in the defect site.^[33] Additionally, because the antibacterial activity of HT-PP was valid through overnight incubation, it

could be useful in adverse conditions when the patient has gotten an infection and does not use any antibiotic or antiseptic agent after implantation for up to 24 h.

After showing the antibacterial activity of coatings, the bacterial populations on the coatings were stained with crystal violet and visualized with fluorescence microscopy. To prevent implant-associated infections, inhibiting biofilm formation is another critical requirement, and fluorescent staining was used to monitor biofilm formation. As seen in the 2D and 3D Z-Stack fluorescent images of the bacterial samples in Figure 4, the coatings caused a considerable decrease in bacterial accumulation on the surface, indicating the critical antimicrobial features of the recent formulation (Figure 4).

2.4. Regulation of Osseointegration

2.4.1. *In Vitro* Biomineralization

Besides the antibacterial activity, an effective implant coating should support the attachment of cells onto the implant surface. Rather than relying on chemical modifications, cellular growth, and proliferation can be augmented by increasing the branching sites on pectin networks.^[11] To prove the adhesive properties of the coating, we seeded osteoprogenitor SaOS-2 cells onto PP and gelatin-coated surfaces and incubated the cells for 1 and 5 h. At the end of defined incubation periods, cells showed a comparable attachment to PP coating and gelatin, a type of positive for cellular attachment, and the difference was only ≈ 3 -fold. This observation proved the adhesive property of the multi-layered coating (Figure S9, Supporting Information).

After showing the adhesive properties of the coating, we intended to analyze the osseointegration capability of the multi-layered coating. The osseointegration process follows similar pathways to osteogenesis, and therefore similar biochemical cues can be monitored to determine the level of tissue maturation around the implant. Mineralizable matrix maturation, biomineralization, and osteoblast/odontoblast differentiation are crucial steps in the osseointegration process. The pectin-peptide gel was employed to provide a mineralizable matrix supporting the biomineralization process, and the fullerene-HT conjugate was used as a phosphatase mimic for the generation of inorganic phosphates (P_i).

The osseointegration capability of hydrogel coatings and biomineralization induction capacity were evaluated with osteoprogenitor SaOS-2 cells. Initially, cytotoxicity testing was done with the cells seeded onto HT-PP coatings and control groups (Figure S8, Supporting Information). PP and HT-PP caused a minor decrease in viability, which could be attributed to early phase differentiation triggered by these groups. Throughout the remainder of the study, it was observed that the cells remained viable. After proving that the coating is not cytotoxic, the level of biomineralization was monitored by Alizarin Red staining (Figure 5). The efficiency of the complete coating was compared to PP gel or only pectin gel, and the performance of the complete coating is exceptional in that these coatings were able to induce biomineralization at day 3 in the absence of osteogenic supplements. An osteogenic supplement or osteogenic medium is commonly used in osteogenesis studies, and the recently reported

scaffold could be able to induce biomineralization without the help of any additional soluble support. HT-PP has been found to be the best among the treatment groups indicating the significance of synergistic effect among the bioactive layers.

2.4.2. Regulatory Effect on Alkaline Phosphatase Expression

The expression profile of alkaline phosphatase (ALP) is a crucial biomarker for detecting the maturation phase of osteogenesis and understanding the influence of implant coatings on ALP protein expression (Figure 6). On day 3, the level of ALP was found to be upregulated for all treatment groups compared to the control. This result indicates that all pectin-containing groups induce osteoblast maturation simultaneously at the early phase of differentiation. Interestingly, on day 7, the ALP level of pectin was highest compared to the other test groups. This observation can be attributed to the phosphatase activity of HT-PP, which might decrease the need for ALP expression. Another reason could be the level of matrix maturation. According to mineralization results, HT-PP leads to the highest mineral deposition, which can be considered faster osteogenesis maturation. After completion of the maturation process, the expression of ALP starts to be downregulated by the feedback mechanisms to prevent over-calcification. Hence, on day 7, the ALP expression level of the HT-PP treated group fell behind the other groups. Another interesting finding of this study was that pectin has a minor osteoinduction capacity, which can be improved by suitable modifications.

2.4.3. Gene Level Guiding of Osteoblast Differentiation

Osteogenic differentiation is driven by regulated changes in the expression of osteogenic marker genes. In the early phase of osteogenesis, the runt-related transcription factor-2 (Runx2) is essential for osteogenic commitment,^[34] and ALP regulates the formation of P_i during the biomineralization process.^[35] The collagen-I (COL-1) expression is upregulated during the proliferation/maturation phase.^[36] Therefore, osteogenic commitment profiles of recently developed coatings were evaluated concerning their ability to induce the expression of Runx2, COL-1, and ALP osteogenic factors (Figure 7).

On day 3, statistically significant enhancements were obtained for early phase differentiation markers. Cells cultured on HT-PP exhibited a better Runx2, COL-1, and ALP expression profile compared to other treatment groups and non-treated control group. The PP group showed less efficiency than the complete design, which can be attributed to the phosphatase-like activity of HT enzyme mimics. Previous studies have shown that phosphatase enzyme results in both increases in osteoblast-specific gene expressions and inorganic phosphate formation. Cleaved inorganic phosphates form calcium phosphate ions on the ECM for tissue formation and mineral formation also promotes gene expression.^[37] Furthermore, enzyme kinetic investigations (Figure 2) indicated that the combination of HT and PP resulted in enhanced enzyme-like activity through a synergistic interaction. Combinatory use of enzyme mimic and fibrous network can be considered as the reason for the improved osteoblast differentiation profile of the HT-PP group. It has also been

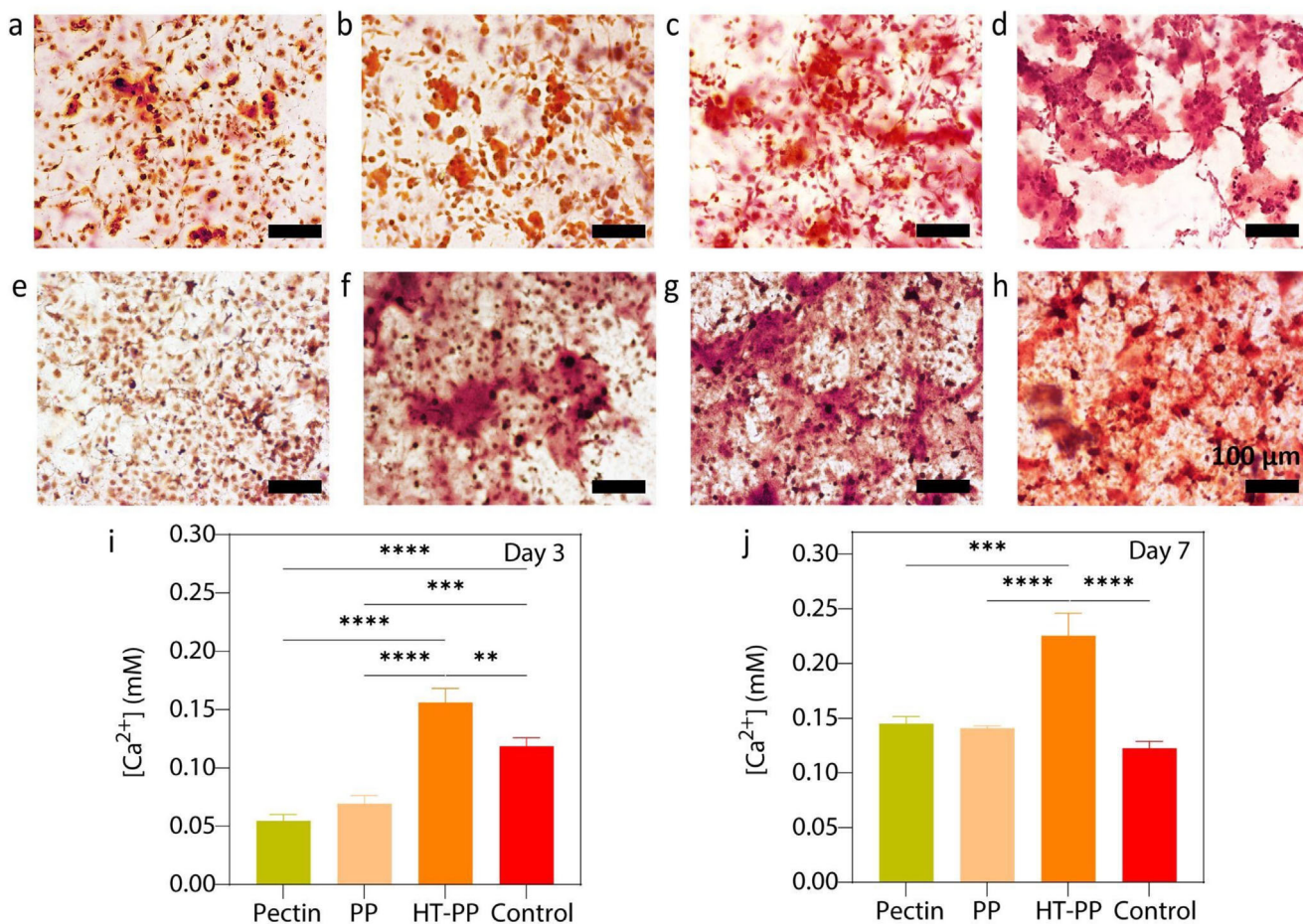


Figure 5. Quantification of Ca²⁺ crystals stained with Alizarin red. a–d) Day 3 and e–h) day 7 mineralization photographs of cells seeded on the coating materials. a and e) Control, untreated SaOS-2 cells. Mineral deposition of SaOS-2 cells seeded on b and f) pectin coating c and g), PP coating and layer-by-layer coating of d and h) HT-PP. i and j) Quantitative results of mineral deposits were determined by their dissolution in cetylpyridinium chloride for (i) day 3 and (j) day 7 (Mean ± SEM, n = 3, one-way analysis of variance (ANOVA); *p < 0.0332, **p < 0.0021, ***p < 0.0002, ****p < 0.0001).

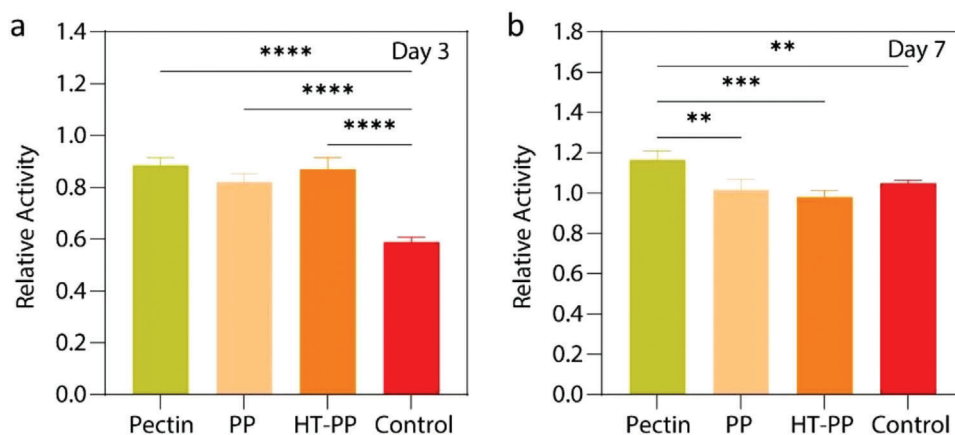


Figure 6. ALP-assay acquired by measurement of released ALP into growth media is shown for a) day 3 and b) day 7 (Mean ± SEM, n = 3, one-way analysis of variance (ANOVA); *p < 0.0332, **p < 0.0021, ***p < 0.0002, ****p < 0.0001).

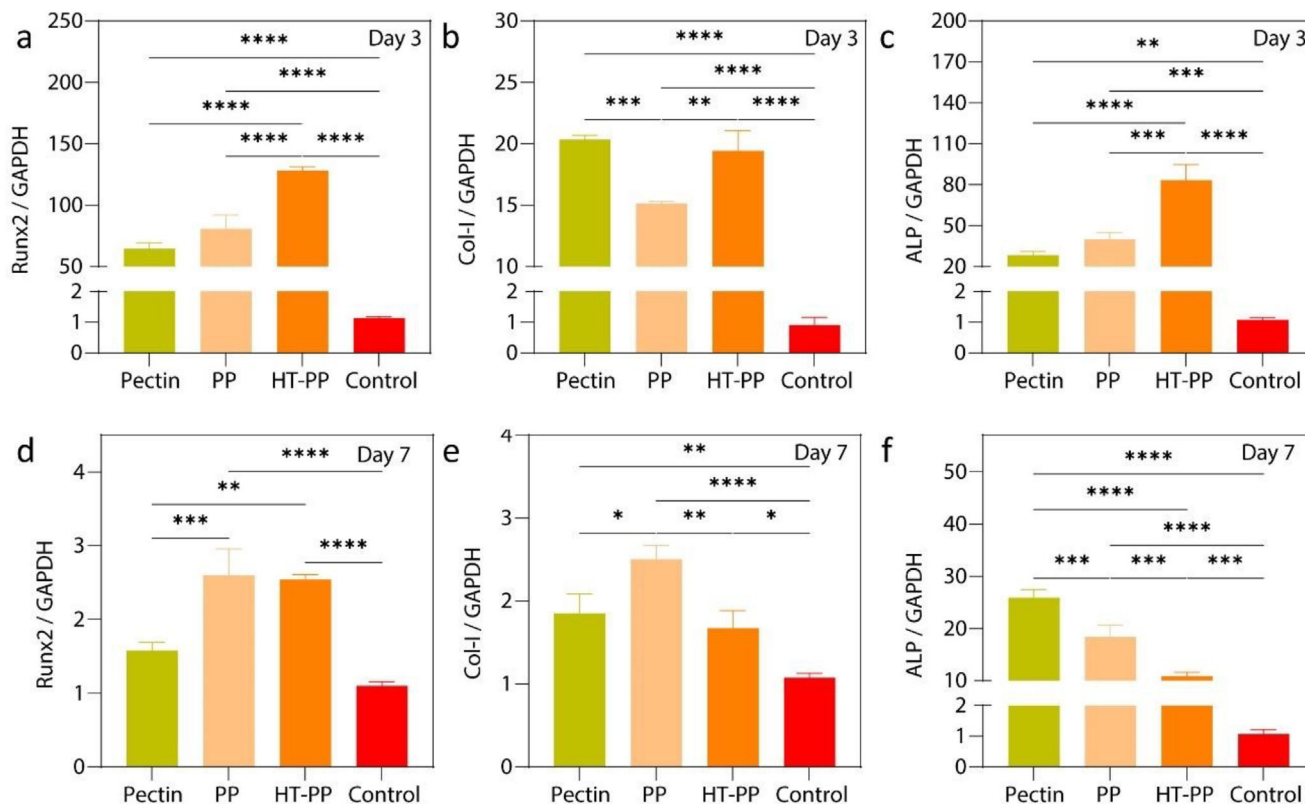


Figure 7. Relative mRNA levels are shown for different markers and different coating materials. Expression levels are given for the early osteoblast marker; a and d) Runx2; Runt-related transcription marker, b and e) Col1; Collagen type 1, and c and f) ALP; Alkaline phosphatase (Mean \pm SEM, $n = 3$, one-way analysis of variance (ANOVA); * $p < 0.0332$, ** $p < 0.0021$, *** $p < 0.0002$, **** $p < 0.0001$).

previously shown that pectin and peptide support osteogenic differentiation.^[32] The synergistic effect of each component of dental coating resulted in notable gene expression levels via enzymatic and structural promotion.

By day 7, gene expressions showed a decrease, indicating the osteoblast maturation process. The HT-PP group was found to be mostly downregulated, providing further evidence of osteoblast maturation, with a decrease in osteogenic differentiation-specific factors (Figure 7). The PP group showed a decrease in gene expression as well, but the level obtained was comparatively higher than the HT-PP group. The results indicate that the use of both enzyme mimic and fibrous network together can enhance the maturation of osteoblasts and that the absence of the enzyme mimic can cause a slight delay in osteoregeneration, emphasizing the importance of each layer.

The recently designed multi-component nanoscale matrices revealed critical properties to develop multifunctional implant coatings. The designed ECM-like matrices significantly reduced microbial load, induced biomineralization, and conducted osteogenic differentiation. Full-layer coating HT-PP exhibited the best profile among the test groups indicating the necessity of complementary interactions between segments.

3. Conclusion

The designed multiple coating system, providing the cells with pectin, peptide amphiphiles, and phosphatase mimicking

HT fullerene nanocatalysts, caused increased osteoinduction of SaOS-2 cells, which is evident from the significantly enhanced mineralization and expression of osteogenic marker genes of the cells grown on multi-layered coating. This enhancement of osteoinduction is caused by the ECM-mimicking nature of the coating and increased P_i concentration owing to the phosphatase activity of the HT nanocatalyst. In addition to raising the osteoinduction, the multi-layered coating had significant antibacterial activity against the gram-negative *E. coli* and gram-positive *B. subtilis* species. With these two indispensable properties required for enhanced osseointegration and decreased risk of infection, our multiple-coating system can be used in dental implants to increase the efficiency of the applied therapies and the comfort of patients.

4. Experimental Section

Materials: Fullerene extract (>70%) was purchased from Tokyo Chemical Industry. Tetra-n-butylammonium hydroxide (40% w/w aq. soln.) was purchased from Alfa Aesar. N,N-Dimethylaminopyridine (DMAP), N,N-dimethylformamide (DMF), penicillin-streptomycin (PS), L-glutamine, alizarin sulfonate sodium (Alizarin red S), Trizma base (>99.9%), L-histidine (>99%), paraformaldehyde, methanol, cetylpyridinium chloride, and crystal violet were purchased from Sigma-Aldrich. Toluene, 2-propanol, diethyl ether, dichloromethane (DCM), pyridine, phosphate-buffered saline (PBS) tablets, and dimethyl sulfoxide (DMSO) were purchased from VWR Chemicals. The alamarBlue cell viability reagent and p-nitrophenyl phosphate (pNPP) were purchased from Invitrogen by

Thermo Fisher Scientific. Runx2, Col-I, ALP, and GAPDH primers were purchased from Sentebiolab. Dulbecco's modified Eagle's medium (DMEM) was purchased from Biowest. Fetal bovine serum (FBS) and trypsin-EDTA were purchased from Biological Industries. Phosphate-buffered saline (PBS, 1x) sterile-filtered was purchased from Gibco. E.Z.N.A. Total RNA Kit I was purchased from Omega Bio-tek. TB Green PrimeScript One Step RT-PCR Kit was purchased from Takara Bio. Pectin was commercially obtained from ABH company. Gelatin was purchased from Bio-Rad. Bovine Serum Albumin (BSA) was purchased from Sigma-Aldrich. Tryptic Soy Agar (TSA) was purchased from Oxoid. Mueller Hinton Broth (MHB) was purchased from Biolife Italiana. Collagen Type-I was purchased from BUGAMED.

Chemical Synthesis of Peptides: Peptide amphiphile molecules were manually synthesized using a standard Fmoc-protected solid phase peptide synthesis method.^[36,37] The synthesized peptide amphiphiles were characterized with quadrupole time-of-flight mass spectrometry (Q-TOF MS) (Agilent 6530 Q-TOF mass spectrometer equipped with an electrospray ionization source (Santa Clara, CA, USA)) and RP-HPLC (Varian ProStar HPLC System).

Synthesis, Activation, and Characterization of Fullerene Enzyme Mimic: Fullerene, the polyhydroxylated derivative of fullerene, was prepared by the previously reported method.^[38] Briefly, fullerene C₆₀ was mixed with hydrogen peroxide (H₂O₂) and sodium hydroxide (NaOH) under grinding conditions in the air at room temperature. This provides water-soluble fullerene after binding many hydroxyl groups to the carbon scaffold. Then, the active fullerene molecules were dissolved in anhydrous dimethylformamide, and the resulting solution was sonicated in the nitrogenous atmosphere for half an hour. The solution was stirred at room temperature in the presence of nitrogen for 30 h. During this time, the solution was sonicated for 1 h with 8-h periods. At the next stage, cold diethyl ether was added to the solution, and the resulting precipitate was separated and washed with diethyl ether two more times. After washing, the solid was dissolved in methanol-containing dichloromethane, and the resulting solution was centrifuged at 5000 rpm for 4 min. After centrifugation, the supernatant was discarded, and the dichloromethane remaining in the pellet was evaporated.^[38] Histidine and threonine amino acids were conjugated to the fullerene surfaces using the previously reported method.^[39] After the synthesis, the synthesized molecule was characterized by H-NMR spectroscopy (Bruker Spectrospin Advanced DPX 400 spectrometer) (Figure S2, Supporting Information).

Preparation of Surface Coating: The first layer of coating, consisting of pectin as a polymeric material with antibacterial properties, biodegradability, and biocompatibility, allows electrostatic interactions with the cationic structure of peptide nanofiber, increases the surface interaction owing to its viscous structure and was suitable for coating. The pectin solution used in the coating was prepared by dissolving pectin in distilled water at a concentration of 2% (w/v).

The second layer was formed by peptide (C₁₂VVAGK-Am peptide) that will induce the formation of the hydrogel by providing the stability of the coating with the interactions with the anionic pectin parts. Positively charged peptides induce non-covalent crosslinking of negatively charged pectin, forming hydrogels that serve as an antibacterial agent and biomineralization matrix. In distilled water, the peptide solution was prepared as 1% (w/v) C₁₂VVAGK-Am peptide. In the third layer, the fullerene nanocatalyst forms the final component of the multilayer as an alkaline phosphatase-like catalyst. The nanocatalyst solution was prepared by dissolving 8.425 mg histidine and threonine-containing fullerene nanocatalyst in 4 mL ultrapure water.

For the viability tests, coatings were prepared on 96-well microplates. 40 μ L pectin and 25 μ L peptide solution were added and left for 2 h in flow conditions until gelling was completed. After the completion of gelling, 1.5 μ L of the required nanocatalyst was added as the last layer and left in laminar flow overnight (\approx 15 h) to dry and form a thin film structure.

The coatings were prepared on spherical glass slides or molds in 24-well microplates for the mineralization and antibacterial activity tests, respectively. 120 μ L pectin and 75 μ L peptide solution were added and left for 2 h in flow conditions until gelation was completed. Then, 15 μ L of the re-

quired fullerene derivative was added as the last layer and left in laminar flow overnight (\approx 15 h) to dry and form a thin film structure.

Scanning Electron Microscopy/EDX: The surface morphology and elemental composition of the composite structure and mineralized surfaces were determined using a SEM combined with EDX. After preparing the coating samples and the ethanol exchange application, the sample was dried with a critical point dryer (CPD). While samples were prepared for CPD, the coating was prepared on the glass slide in a 24-well plate as described above. Afterward, a 5-stage ethanol exchange protocol was applied. 25%, 50%, 75%, and 95% ethanol solutions were added to the coating for 5 min and then discarded. Finally, 100% ethanol was added, incubated for 10 min, and discarded. The remaining were kept in 100% ethanol until CPD.^[40] Measurements for three independent coatings were performed using ZEISS Gemini SEM. Where necessary, samples were coated with 3 nm Au/Pd.

Rheometer Analysis: The network structure formation at pH 7.4 with and without cells was studied by oscillatory rheology. An Anton Paar Physica RM301 Rheometer operating with a 12 mm parallel plate configuration was used to probe the structural gel properties of the cell, pectin, and peptide gel network. Samples were prepared by mixing 2% pectin and peptide in distilled water with a total volume of 250 μ L. A gap distance of 0.5 mm was used with 10 rad s⁻¹ angular frequency and 0.1% shear strain.^[37]

Fourier Transform Infrared Spectroscopy: FTIR determined the functional groups and cross-linking in compounds. The FTIR analysis spectra were recorded in the transmittance mode using an ATR-Nicolet iS10 Spectrometer (Thermo Fisher Scientific Inc.) using the deuterated triglycine sulfate KBr method for the measurements. For all the spectra recorded, the samples underwent a 32-scan data accumulation in the range of 400–4000 cm⁻¹ at a spectral resolution of 4.0 cm⁻¹.

X-Ray Diffractometry: The stainless-steel surface was coated with 200 μ L pectin and peptide solution and placed in 6-well plates. 480 mM CaCl₂ and 288 mM β -glycerophosphate (β -gly) dissolved in distilled water were added to each well to initiate the mineralization process. The solution was removed from the surface, and the stainless-steel surface was dried at CO₂ incubator conditions for 7 days before analysis.^[37] The crystallographic structure of calcium phosphate crystals was evaluated with a PAN analytical Empyrean X-ray diffractometer using Cu K α radiation. Pectin and peptide-coated stainless-steel surfaces were prepared as described and measured without further modification. The rotation time was 16 s, the scan range was from 20° to 70°, and the step size was 0.0525°. The planes observed were (111) and (211) for all of the crystals formed on surfaces.

Optical Profilometry: Surface roughness was an important aspect of a machined part and greatly affects its performance. The coatings on the stainless-steel surface were prepared as previously mentioned. The surface roughness was measured using a Profilm 3D microscope using white light interferometry (WLI), which was a measurement technique to obtain a 3D scan.

Contact Angle Measurements: As already mentioned, coatings on the stainless-steel surface were made, and water was added to the blank stainless-steel surface. The surfaces were compared in terms of contact angle and surface adhesiveness.^[41] The contact angle was tested on a KRÜSS DSA1 (Biolin Scientific, Attention-Theta) by static drop method with 3 μ L water per drop. The values were reported by version 1.80 analyzer of drop shape.^[42]

Stability Testing: HT-PP coatings were prepared on different surfaces that were polystyrene coverslips, stainless-steel plates, glass microscope slides, and swimming molds, using 80 μ L pectin, 50 μ L peptide, and 15 μ L HT solutions. The weight of the coated and uncoated surfaces was measured. Coated surfaces were waited in 1x PBS for 15 or in dH₂O for 20 days. When the desired incubation time finished, coatings were dried in laminar flow and the final weight was found. Percent weight loss was calculated with the following equation; Weight loss percent = (initial weight – final weight) \times 100 / initial weight.

pNPP Hydrolysis Assay: HT-PP coatings were made inside the wells of a 96-well plate, and as the control groups, pectin, peptide amphiphile, and HT was added to wells in the amount used for coatings. As the reaction buffer, tris-HCl pH 8.8 was used and the volume inside the wells was

completed to 192 μL . 8 μL 0.1 M pNPP solution dissolved in the reaction buffer was added just before the absorbance reading and the kinetic reads were taken at 405 nm wavelength, at 37 $^{\circ}\text{C}$, for 10 min using BioTek SynergyH1 microplate reader. A group containing only the reaction buffer and pNPP solution was used as the blank.

Antibacterial Activity Assay: Bacteria seeded by the scratch smear method on TSA were incubated overnight at 37 $^{\circ}\text{C}$. After incubation, one colony was inoculated to 3 mL MHB and incubated overnight at 37 $^{\circ}\text{C}$. 100 μL from the first liquid culture was added to a fresh 3 mL MHB. Bacteria at the mid-log phase were diluted to a concentration of 2×10^6 with MHB. 1 mL diluted bacterial solution was added to the wells of a 24-well plate containing 1 mL sterile MHB and mold with antibacterial coating or collagen coating. The plate was incubated for 16 h at 37 $^{\circ}\text{C}$ with 30 rpm shaking. After the incubation, the solutions were discarded, and the wells were washed twice with 1 \times PBS. 1 mL 10% Alamar Blue Assay reactant was added to the wells and incubated for 1 h at 37 $^{\circ}\text{C}$ with 100 rpm shaking. At the end of 1 h, fluorescence coming due to the alive bacteria inside the coating was measured at 560–590 nm.

Bacterial Fixation and Microscopy: After the incubation process mentioned above was completed, the bacterial cells were fixed in 4% paraformaldehyde for 15 min at room temperature and then washed twice with 1 \times PBS. Then, the fixed cells were stained with 0.025% crystal violet solution (20% methanol and 80% distilled water) and visualized with a fluorescent microscope at 550–590 nm (ZEISS Axio Observer 7).

Bacteria Colony Counting Assay: The pour plate method was done with some changes from Basic Practical Microbiology, a Manual by Society for General Microbiology (SGM). Bacterial solutions on the coated plates were incubated overnight, and after incubation, solutions were completely removed from the wells with a swab and taken into TSB. After that, serial dilutions were done. Serial dilutions were obtained up to 1:100,000 and were inoculated on TSA as two replicates for each dilution. Then, the petri dishes were incubated overnight at 37 $^{\circ}\text{C}$, and the colony count was performed on the following day using ImageJ software. Calculations were done by using the formula given below.

$$\text{CFU/mL} = \text{CFU} \times \text{dilution factor} \times 1/\text{aliquot} \quad (1)$$

Cell Culture and Maintenance: SaOS-2 human osteosarcoma cells were used for in vitro cell culture experiments on coated culture surfaces. All cells were cultured and propagated in 75 cm^2 cell culture flasks using DMEM supplemented with 10% FBS, 1% penicillin/streptomycin, and 2 mM L-glutamine. Cells were grown at 37 $^{\circ}\text{C}$ in a humidified chamber supplied with 5% CO_2 .

Cellular Viability: The viability of SaOS-2 cells was analyzed on HT-PP, PP, and pectin-coated culture plate surfaces at 24 and 48 h. Cells were seeded onto coated tissue culture plate surfaces in DMEM supplemented with 10% FBS, 2 mM L-glutamine, and 1% penicillin/streptomycin at a density of 15×10^3 cells/well. After the required incubation times, the viability of the cells on coated and control surfaces was quantified by Alamar Blue assay by measuring absorbance values at 570 nm (background absorbance was at 590 nm, Biotek Epoch 2 Microplate Spectrophotometer was used). The viability of cells on the coated surface was normalized to that of cells on bare surfaces.

Cellular Adhesion and Proliferation Assay: Cellular adhesion was evaluated by adding 15×10^3 cells (4 replicas for each sample) to 2% (w/v) gelatin on a glass slide and PP coating on 24-well plates, using a serum-free medium that contains 7 mg mL^{-1} of BSA. Before seeding, the cells were incubated in an adhesion medium for 1 h and taken to the coating. After 1 and 5 h of incubation, the wells were washed with 1 \times PBS, and the adhering cells were imaged using microscopy. The counting of the cells was performed using the ImageJ application. Cellular adhesion was compared with gelatin (control group).

Cellular Mineralization and Alizarin Red Staining Assay: Biomineralization and calcium phosphate tests with SaOS-2 cells were carried out on coated well plates. SaOS-2 cells were seeded on 24-well plates at a density of 6×10^4 cells/well in DMEM with 10% FBS. The medium of the cells was replaced with a fresh culture medium containing 10% FBS/DMEM once in 2 days. Calcium deposition on the surfaces was measured on days 3 and 7

using Alizarin Red as a quantitative colorimetric staining method. Briefly, cells were fixed with ice-cold ethanol for 30 min and stained with 40 mM Alizarin-Red Stain for 30 min. After washing 1–2 times with 1 \times PBS to remove nonspecific Alizarin-Red binding, cells were imaged with an optical microscope. Alizarin Red-bound calcium extraction was performed by using 10% (w/v) cetylpyridinium chloride in 10 mM sodium phosphate (pH 7) for 20 min at room temperature, and the concentration of Alizarin-Red S was determined by measuring the absorbance at 555 nm (Biotek Epoch 2 Microplate Spectrophotometer).

Gene Expression Analysis: For RNA isolation, the coatings were prepared in a 24-well plate on a glass slide so that there were 6 copies for each group. (pectin, PP, HT-PP). SaOS-2 cells were seeded at a density of 55×10^3 cells/well on the coating surface, and total RNA was isolated using E.Z.N.A. Total RNA Kit I according to manufacturer's instructions. The yield and purity of extracted RNA were assessed by Take3 (Biotek Epoch 2 Microplate Spectrophotometer). cDNA synthesis from RNA and qRT-PCR was performed using TB Green PrimeScript One Step RT-PCR Kit according to the manufacturer's instructions. The gene expression profiles of cells during osteogenic differentiation were assessed by quantitative RT-PCR (qRT-PCR) analysis (Bio-Rad CFX96TM C1000 Touch Thermal Cycler). The expression profiles of RUNX2, Col 1, and ALP were analyzed for SaOS-2 cells. The reaction efficiencies for each primer set were evaluated with a standard curve using 5-fold serial dilutions of total RNA. Primary gene expression results were normalized to the expression level of GAPDH for the expression data analysis. A comparative cycle threshold method was used to analyze the results.

ALP Assay: Before RNA isolation, cellular alkaline phosphatase activity was determined with 2 samples collected from cell surfaces. Enzymatic activity was evaluated by treating the medium with the 5 mM substrate analog pNPP. The groups were prepared to be 4 replicates with and without substrates in 96 well plates, and DMEM was used as blank. The groups containing substrates were prepared as 80 μL samples and 50 μL pNPP, and the groups without substrates were prepared as 130 μL samples. After incubation at room temperature for 20 h and at 37 $^{\circ}\text{C}$ for 1 h protected from light, a 410 nm absorbance measurement was taken, and the results were evaluated (Biotek Epoch 2 Microplate Spectrophotometer).^[43,44]

Statistical Information: Sample replicates for the studies were determined as 4. Differences between groups were determined by one-way ANOVA or two-way ANOVA (analysis of variance using Tukey's post-hoc tests). Results with a p -value of ≤ 0.05 were considered statistically significant. All statistical analyses were performed using GraphPad Prism (v7; San Diego) software.

Supporting Information

Supporting Information is available from the Wiley Online Library or from the author.

Acknowledgements

B.U., Z.D., and O.C. contributed equally to this work. This work was funded by the TUBITAK (The Scientific and Technological Research Council of Turkey) 121M973 fellowship. Graphical Abstract figure was created with BioRender.com. The authors thank Fatmanur Elif Sara, Saliha Ocuz, and Eda Eserozbek for helping with antibacterial activity tests.

Conflict of Interest

The author declares no conflict of interests.

Data Availability Statement

Data available on request from the authors.

Keywords

ECM-mimic, implant coating, osseointegration, pectins, peptides

Received: February 15, 2023

Revised: April 13, 2023

Published online:

- [1] C. Veiga, *Adv. Mater.* **2012**, *32*, 133.
- [2] C. R. Arciola, D. Campoccia, P. Speziale, L. Montanaro, J. W. Costerton, *Biomaterials* **2012**, *33*, 5967.
- [3] Y. C. Shin, J.-H. Bae, J. H. Lee, I. S. Raja, M. S. Kang, B. Kim, S. W. Hong, J.-B. Huh, D.-W. Han, *Biomater. Res.* **2022**, *26*, 11.
- [4] W.-H. Kim, Y. C. Shin, S.-H. Lee, M. S. Kang, M.-S. Lee, J. H. Lee, J.-H. Lee, D.-W. Han, B. Kim, *J Ind Eng Chem* **2022**, *116*, 543.
- [5] R. Rasouli, A. Barhoum, H. Uludag, *Biomater. Sci.* **2018**, *6*, 1312.
- [6] A. Shekaran, A. J. Garcia, *J Biomed Mater Res A* **2011**, *96A*, 261.
- [7] A. Presentato, A. Scurria, L. Albanese, C. Lino, M. Sciortino, M. Pagliaro, F. Zabini, F. Meneguzzo, R. Alduina, D. Nuzzo, R. Ciriminna, *ChemistryOpen* **2020**, *9*, 628.
- [8] K. Gurzawska, R. Svava, Y. Yihua, K. B. Haugshøj, K. Dirscherl, S. B. Lavery, I. Byg, I. Damager, M. W. Nielsen, B. Jørgensen, N. R. Jørgensen, K. Gotfredsen, *Mater Sci Eng C Mater Biol Appl.* **2014**, *43*, 117.
- [9] R. Ciriminna, A. Fidalgo, F. Meneguzzo, A. Presentato, A. Scurria, D. Nuzzo, R. Alduina, L. M. Ilharco, M. Pagliaro, *ChemMedChem* **2020**, *15*, 2228.
- [10] A. Lapomarda, A. De Acutis, I. Chiesa, G. M. Fortunato, F. Montemurro, C. De Maria, M. Mattioli Belmonte, R. Gottardi, G. Vozzi, *Biomacromolecules* **2020**, *21*, 319.
- [11] F. Munarin, S. G. Guerreiro, M. A. Grellier, M. C. Tanzi, M. A. Barbosa, P. Petrini, P. L. Granja, *Biomacromolecules* **2011**, *12*, 568.
- [12] C. E. Campiglio, A. Carcano, L. Draghi, *J. Biomed. Mater. Res., Part A* **2022**, *110*, 515.
- [13] F. Garavand, M. Rouhi, S. H. Razavi, I. Cacciotti, R. Mohammadi, *Int. J. Biol. Macromol.* **2017**, *104*, 687.
- [14] F. Munarin, P. Petrini, M. C. Tanzi, M. A. Barbosa, P. L. Granja, *Eur Phys J E Soft Matter* **2012**, *8*, 4731.
- [15] M. Goktas, G. Cinar, I. Orujalipoor, S. Ide, A. B. Tekinay, M. O. Guler, *Biomacromolecules* **2015**, *16*, 1247.
- [16] G. Gulseren, I. C. Yasa, O. Ustahuseyin, E. D. Tekin, A. B. Tekinay, M. O. Guler, *Biomacromolecules* **2015**, *16*, 2198.
- [17] D. Yeniterzi, Z. Demirsoy, A. Saylam, S. Özçubukçu, G. Gülseren, *Macromol. Biosci.* **2022**, *22*, 2200079.
- [18] S. Vimalraj, *Gene* **2020**, *754*, 144855.
- [19] Y. Murakami, J.-I. Kikuchi, Y. Hisaeda, O. Hayashida, *Chem. Rev.* **1996**, *96*, 721.
- [20] G. Gülseren, A. Saylam, A. Marion, S. Özçubukçu, *ACS Appl. Mater. Interfaces* **2021**, *13*, 45854.
- [21] Z. Demirsoy, G. Gulseren, *ACS Appl. Nano Mater.* **2022**, *5*, 14285.
- [22] T. Li, H. C. Dorn, *Small* **2017**, *13*, 1603152.
- [23] E. Arslan, I. C. Garip, G. Gulseren, A. B. Tekinay, M. O. Guler, *Adv. Healthcare Mater.* **2014**, *3*, 1357.
- [24] R. C. Gaal, B. D. Ippel, S. Spaans, M. I. Komil, P. Y. W. Dankers, *J. Polym. Sci.* **2021**, *59*, 1253.
- [25] C. N. Salinas, K. S. Anseth, *J Tissue Eng Regen Med* **2008**, *2*, 296.
- [26] D. Demir, S. Ceylan, D. Göktürk, N. Bölgen, *Polym. Bull.* **2021**, *78*, 2211.
- [27] S. C. Sartoretto, A. T. Alves, R. F. B. Resende, J. Calasans-Maia, J. M. Granjeiro, M. D. Calasans-Maia, *J Appl Oral Sci.* **2015**, *23*, 279.
- [28] J. Pan, S. Prabaharan, M. Rajan, *Biomed. Pharmacother.* **2019**, *119*, 109404.
- [29] A. Aljabo, E. A. Abou Neel, J. C. Knowles, A. M. Young, *Mater. Sci. Eng. C* **2016**, *60*, 285.
- [30] I.-M. Hung, W.-J. Shih, M.-H. Hon, M.-C. Wang, *Int. J. Mol. Sci.* **2012**, *13*, 13569.
- [31] L. W. Riley, R. E. Blanton, *Microbiol Spectr* **2018**, *6*, 6.6.01.
- [32] C. Uslu, S. Narin, Z. Demirsoy, H. B. Öksüz, G. Gülseren, *Int. J. Biol. Macromol.* **2023**, *233*, 123604.
- [33] L. Zhao, H. Wang, K. Huo, L. Cui, W. Zhang, H. Ni, Y. Zhang, Z. Wu, P. K. Chu, *Biomaterials* **2011**, *32*, 5706.
- [34] C. A. Yoshida, T. Furuichi, T. Fujita, R. Fukuyama, N. Kanatani, S. Kobayashi, M. Satake, K. Takada, T. Komori, *Nat. Genet.* **2002**, *32*, 633.
- [35] M. Ojansivu, S. Vanhatupa, L. Björkvik, H. Häkkinen, M. Kellomäki, R. Autio, J. A. Ihalainen, L. Hupa, S. Miettinen, *Acta Biomater.* **2015**, *21*, 190.
- [36] H. Ceylan, S. Kocabay, A. B. Tekinay, M. O. Guler, *Eur Phys J E Soft Matter* **2012**, *8*, 3929.
- [37] G. Gulseren, I. C. Yasa, O. Ustahuseyin, E. D. Tekin, A. B. Tekinay, M. O. Guler, *Biomacromolecules* **2015**, *16*, 2198.
- [38] P. Chaudhuri, A. Paraskar, S. Soni, R. A. Mashelkar, S. Sengupta, *ACS Nano* **2009**, *3*, 2505.
- [39] G. Gülseren, A. Saylam, A. Marion, S. Özçubukçu, *ACS Appl. Mater. Interfaces* **2021**, *13*, 45854.
- [40] E. R. Fischer, B. T. Hansen, V. Nair, F. H. Hoyt, D. W. Dorward, *Curr Protoc Microbiol* **2012**, *25*, 2B21.
- [41] V. Krishnan, Y. Kasuya, Q. Ji, M. Sathish, L. K. Shrestha, S. Ishihara, K. Minami, H. Morita, T. Yamazaki, N. Hanagata, K. Miyazawa, S. Acharya, W. Nakanishi, J. P. Hill, K. Ariga, *ACS Appl. Mater. Interfaces* **2015**, *7*, 15667.
- [42] H. Li, C. Gao, L. Tang, C. Wang, Q. Chen, Q. Zheng, S. Yang, S. Sheng, X. Zan, *ACS Appl. Bio Mater.* **2020**, *3*, 673.
- [43] D. Jiang, D. Ni, Z. T. Rosenkrans, P. Huang, X. Yan, W. Cai, *Chem. Soc. Rev.* **2019**, *48*, 3683.
- [44] A. Sabokbar, P. J. Millett, B. Myer, N. Rushton, *Bone Miner.* **1994**, *27*, 57.